water

MDPI

Article

Crop Coefficients and Transpiration of a Super Intensive Arbequina Olive Orchard using the Dual K_c Approach and the K_{cb} Computation with the Fraction of Ground Cover and Height

Teresa A. Paço [1,*], Paula Paredes [1], Luis S. Pereira [1], José Silvestre [2] and Francisco L. Santos [3]

1 Research Center on Linking Landscape, Environment, Agriculture and Food (LEAF), Instituto Superior de Agronomia, Universidade de Lisboa, Tapada da Ajuda, 1349-017 Lisboa, Portugal; pparedes@isa.ulisboa.pt (P.P.); lspereira@isa.ulisboa.pt (L.S.P.)

2 Instituto Nacional de Investigação Agrária e Veterinária, I.P. (INIAV), 2565-191 Dois Portos, Portugal; jose.silvestre@iniav.pt

3 Instituto de Ciências Agrárias e Ambientais Mediterrânicas (ICAAM), Universidade de Évora, Largo dos Colegiais, 7006-554 Évora, Portugal; f.lucio.santos@gmail.com

* Correspondence: tapaco@isa.ulisboa.pt; Tel.: +351-21-3653331

Received: 28 January 2019; Accepted: 19 February 2019; Published: 22 February 2019

Abstract: The SIMDualKc model was used to simulate crop water requirements for a super high density olive orchard in the region of Alentejo, Portugal. This model uses the dual crop coefficient approach to estimate and partitioning the actual crop evapotranspiration ($ET_{c\ act}$) and therefore to perform the soil water balance. The model was calibrated with 2011 tree transpiration using trunk sap flow measurements and was validated using similar data from 2012 and tested with 2013 data. Low root mean square errors (RMSE < 0.53 mm·d^{-1}) and acceptable modelling efficiency indicators (EF > 0.25) were obtained. Further validation was performed comparing modelled $ET_{c\ act}$ with eddy covariance measurements. These indicators support the appropriateness of using SIMDualKc to guide irrigation management. The basal crop coefficient (K_{cb}) curves obtained with SIMDualKc for those 3 years were compared with the K_{cb} values computed with the Allen and Pereira approach (A&P approach) where K_{cb} is estimated from the fraction of ground cover and plant height considering an adjustment factor for crop stomatal control (F_r). F_r values were obtained through a trial and error procedure through comparing the K_{cb} estimated with this approach and with SIMDualKc. The K_{cb} curves obtained by both methods resulted highly correlated, which indicates that the A&P approach may be used in the irrigation management practice to estimate crop water requirements. Results of performing the soil water balance with SIMDualKc have shown that soil evaporation is a large fraction of $ET_{c\ act}$, varying between 41% and 45% for the 3 years under study. Irrigation, applied with a drip system, represented 39 to 56% of $ET_{c\ act}$, which shows the great importance of irrigation to achieve the water requirements of super intensive olive orchards. Nevertheless, the analysis has shown that the irrigation management adopted at the orchard produces a water deficit larger than desirable, with a ratio of $ET_{c\ act}$ to non-stressed crop evapotranspiration (ET_c) varying from 70% to 94% during the mid-season, when that ratio for a eustress irrigation management could be around 90%.

Keywords: Evapotranspiration; Irrigation; Density coefficient; Dual crop coefficients; Row crops

1. Introduction

Olive orchards consist of the dominant permanent crops in Portugal, covering approximately 50% of the total area with tree crops, namely in Alentejo, southern Portugal, where olives are mainly cropped for oil production. Super high density olive orchards, with more than 1500 trees ha^{-1}, also known as hedgerow olive orchards, are growing fast due to their high yield and economic productivity [1–3]. However, they have higher water requirements than less intensive orchards [1]; it is therefore necessary to improve related knowledge about crop evapotranspiration to support appropriate irrigation management and scheduling [4,5]. Meanwhile, impacts of water deficit on olives growth and yield are relatively well known [6–11]. That knowledge about olives evapotranspiration and responses to water deficits is also essential to assess scenarios of climate change expected for the region, mainly referring to higher temperature during summer and less rainfall in winter and autumn [12,13].

Although information on crop evapotranspiration can be obtained through using various field measurements techniques [14], those involving direct measurements of ET are generally expensive, labour consuming, require appropriate skills of users and are more appropriate for research, that is, for example, measurements of soil water content [15,16], sap-flow [17–19] and eddy covariance [18–20], which are applied in this study. Differently, crop ET modelling, using commonly observed meteorological data [4], radiometric canopy temperature [21,22], web based sensors networks [23] and remote sensing information [24–28], including using unmanned aerial vehicles [29] might be useful irrigation management tools, namely for irrigation scheduling purposes and to generate mitigation scenarios to face drought and climate change. Example of models applications to olive orchards include WABOL [30], SIMDualKc [19] and HYDRUS 2D [31].

The most common approach to estimate potential crop evapotranspiration (ET_c) is the use of the K_c-ET_o approach [32], where ET_o is the grass reference evapotranspiration (PM-ET_o) and K_c is a crop coefficient, which relates ET_c with ET_o relative to various crop characteristics [4]. K_c changes throughout the crop season and a multi-stage linear approximation is commonly used to represent the K_c curve through defining their values at the initial, mid-season and end-season stages, respectively $K_{c\,ini}$, $K_{c\,mid}$ and $K_{c\,end}$ [4]. Adopting the dual K_c approach, both ET_c components are considered, crop transpiration described by the basal crop coefficient K_{cb} and the soil evaporation described by the coefficient K_e [33]. When any crop stress occurs, K_{cb} is corrected through a stress coefficient, K_s, resulting that the actual K_{cb} ($K_{cb\,act} = K_s\,K_{cb}$) is smaller than the non-stress or standard one, that is, $K_{cb\,act} \leqslant K_{cb}$. It results that the actual crop ET is smaller than the potential, non-stressed ET, that is, $ET_{c\,act} \leqslant ET_c$. Therefore:

$$ET_{c\,act} = (K_s\,K_{cb} + K_e) \times ET_o = (K_{cb\,act} + K_e) \times ET_o = K_s \times K_c \times ET_o = K_{c\,act} \times ET_o \quad (1)$$

Field research, as the one reported in this study, is required to determine K_c and K_{cb} in relation with the crop characteristics and crop management. The standard or non-stressed values of K_{cb} and K_c are transferable to other locations—where training of olives orchards are similar—after adjusting K_c or K_{cb} to the prevailing climate conditions as proposed by Allen et al. [4]. The use of a well calibrated model such as SIMDualKc [34], which adopts the dual K_c approach to partitioning $ET_{c\,act}$ into actual plant transpiration and soil evaporation, using respectively $K_{cb\,act}$ and K_e [4,33], is quite helpful to accurately computing $ET_{c\,act}$ and to derive the standard K_{cb} and K_c values as demonstrated in previous studies [35–37]. Moreover, the performance of that partition using SIMDualKc has been positively tested through comparing the model simulated transpiration against sap-flow measurements [19,38,39] or the simulated soil evaporation against micro-lysimeters' observations [40–42].

In alternative to modelling, Allen and Pereira [43] proposed predicting K_{cb} or K_c by adopting a density coefficient (K_d) computed from the fraction of ground cover (f_c) and the crop height (h), herein referred as A&P approach. It takes into consideration crop stomatal control through an adustment factor (F_r) that varies with crop characteristics and water management. The A&P approach has

been used to ease the SIMDualKc modelling process applied to partial cover woody crops, such as vineyards [35], peach orchards [38] and olive orchards [19]. However, the A&P approach has not yet been used extensively for predicting K_{cb} throughout the crop season.

Considering the analysis above, the objectives of this study consisted of (i) calibrating and validating the model SIMDualKc using both sap-flow estimates of transpiration and ET eddy covariance observations; (ii) determining K_{cb} and K_c from SIMDualKc calibration; (iii) testing the A&P approach for predicting K_{cb} from the fraction of ground cover and crop height; and (iv) determining the terms of the soil water balance, particularly relationships between soil evaporation, actual transpiration and $ET_{c\,act}$. The overall objective is to provide information for irrigation of olives' orchards with reduced irrigation, so accepting a yield-water beneficial stress, the "eustress."

2. Material and Methods

2.1. Experimental Site

The experimental site (38°24'N, 7°43'W, 143 m a.s.l.) is located in Alentejo, Southern Portugal, in a commercial super-high intensive hedgerow olive orchard farmed by "Olivais do Sul." The orchard has a total area of 78 ha, which land has a smooth undulation. The climate is dry sub-humid of Mediterranean type, with most of the rainfall in autumn and winter; according to the Köppen-Geiger classification [44], the climate is a Csa, characterized by mild rainy winters and dry hot summers. The annual rainfall ranged between 511 and 736 mm in the experimental years, while the average monthly temperature ranged from 9.6 °C in January to 23.3 °C in July and August. Prevailing winds are from the North-West direction. Main daily weather data characterizing the experimental years is presented in Figure 1.

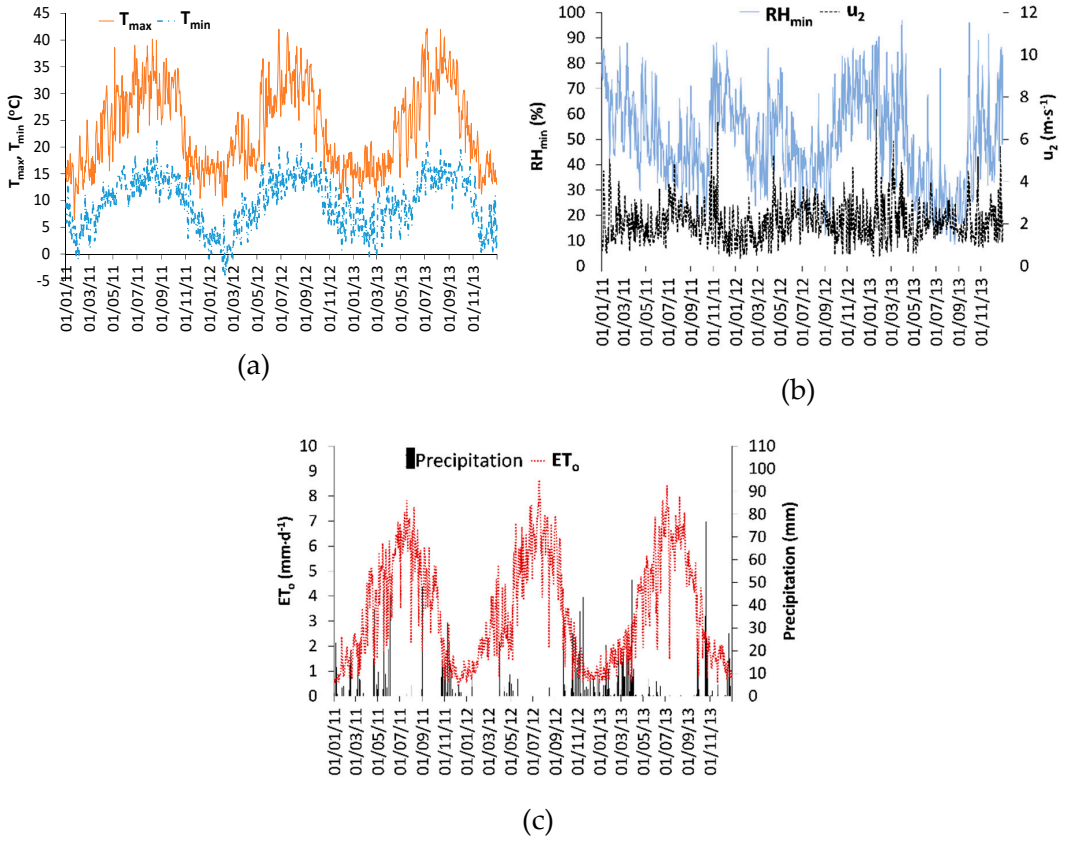

Figure 1. Daily weather data of Viana do Alentejo relative to (**a**) maximum (T_{max}) and minimum (T_{min}) temperatures, (**b**) minimum relative humidity (RH_{min}), wind speed at 2 m height (u_2) and (**c**) precipitation and reference evapotranspiration (ET_o) for the period 2011–2013.

The soil is a Cambissol [45] having a sandy loam texture, with moderate to low infiltration. Soil water at field capacity averages 0.24 $cm^3 \cdot cm^{-3}$ through the soil profile down to 1.20 m, while the permanent wilting point to the same depth is 0.12 $cm^3 \cdot cm^{-3}$. The total available water to that depth is TAW = 160 mm. Soil water observations were performed weekly with a TDR probe (TRIME, IMKO, Ettlingen, Germany); data were used to perform the soil water balance considering a soil root zone depth Z_r = 1.10 m.

The olive trees (cv. Arbequina) were hedgerow planted in 2006 adopting a super-high density (1.35 m × 3.75 m, 1975 trees ha^{-1}). The observed crop growth stages dates along the crop seasons of 2011, 2012 and 2013 are presented in Table 1. The fraction of ground cover (f_c, dimensionless) was estimated from measurements of the crown diameter along the row direction and perpendicularly to it for 51 trees. In addition, f_c values estimated from remote sensing [28] were also considered. f_c ranged from 0.17 to 0.38. The tree height (h, m) ranged from 3.0 to 4.0 m. Both f_c and h varied through the crop season because trees were pruned during winter, by early January. However, in 2012, after a severe frost that occurred by late February, a heavy pruning was applied after, which caused larger changes in f_c and h in that year. Harvesting in the study plots were performed by 16 October in 2011 and 2012 and by 10 October in 2013 (Table 1). The yield average was 14 ton·ha^{-1} in 2011 and 18 ton·ha^{-1} in 2013. A low yield of 3 ton·ha^{-1} was observed in 2012 due to the referred frost and heavy pruning.

Table 1. Crop growth stages of the olive orchard under study.

Year	Crop Growth States					
	Non-Growing	**Initiation**	**Crop Development**	**Mid-Season**	**Late-Season**	**Non-Growing**
2011	1/1–28/2	1/3–15/3	16/3–30/4	1/5–13/9	14/9–11/11	12/11–31/12
2012	1/1–20/3	21/3–11/4	12/4–14/5	15/5–10/9	11/9–23/11	24/11–31/12
2013	1/1–2/3	3/3–17/3	18/3–20/4	21/4–19/9	20/9–15/11	16/11–31/12

Ground cover conditions affecting soil evaporation may be taken into consideration in the water balance simulations by SIMDualKc and were therefore observed. They refer to both crop residues and active ground cover [34,35,46]. In 2011, a reduced active ground cover was present from early January until May, covering 10% of the ground in the row and 5% in the inter-row. In 2012, following the frost by February, a heavy defoliation occurred and leaves formed an organic mulch from late February until early August; its ground cover fraction was estimated as 0.30, corresponding to a reduction of the soil evaporation of 30%. In 2013, an active ground cover of nearly 20% on both the row and the inter-row was observed from January until May, when it dried out and became a residues cover.

Irrigation took place nearly every day during spring and summer and was applied by the evening. A drip system was used, with emitters spaced of 0.75 m along the row. The emitters discharge was of 2.3 L h^{-1}. The wetted fraction (f_w = 0.23) was calculated from the area of a wetted ellipse circling each emitter. Irrigations were scheduled by the farmer, who adopted average daily irrigation depths close to 3 mm, however varying from 1 to 8 mm, approximately. Irrigation depths were measured with a tipping-bucket rain gauge (ARG100, Environmental Measurements Ltd., Sunderland, UK).

2.2. Eddy Covariance Measurements

The eddy covariance (EC) micrometeorological technique was used to measure evapotranspiration during short periods of the irrigation season (July–August in 2011 and June–August in 2012) as a strategy to calibrate the sap flow measurements and obtaining accurate transpiration estimates. This strategy has been successfully used in previous studies [38,47].

The EC system comprised a three-dimensional sonic anemometer and a krypton hygrometer (respectively Models CSAT3 and KH20, Campbell Scientific, Inc., Logan, UT, USA) mounted at a height of 4.8 m on a metallic tower, with a path separation of 0.1 m. The fetch were 470 m, 353 m, 455 m and 504 m for the north, west, south and east directions, respectively (Figure 2). EC raw data (H—sensible heat flux density and LE—latent heat flux density) were collected at a 10 Hz frequency to a datalogger

(Model CR1000, Campbell Scientific, Inc., Logan, UT, USA) and afterwards analysed with the Software package TK3 [48] for correction and calculation of 30 min-averages. Data corrections were performed according to Foken et al. [49]. They included: despiking of the raw data [50]; coordinate rotation using the Double Rotation method [51] to account for the non-flat terrain conditions; corrections for oxygen cross-sensitivity of the krypton hygrometer [52] and spectral loss [53]; conversion of buoyancy flux to sensible heat flux [54]; and the WPL correction for density fluctuations [55]. To evaluate the surface energy balance, soil heat flux (G) and net radiation (R_n) were measured using eight soil heat flux plates (calibrated Peltier modules sealed 20 V, 4.4 A, 40 × 40 × 3.9 mm, RS Components, Madrid, Spain) and a net radiometer (Model NR-LITE, Campbell Scientific, Inc., Logan, Utah, USA), respectively. The soil heat flux plates were placed in the tree row and in the inter-rows at a depth of 2 cm. The daily energy balance equation error closure was determined by linear regression forced to origin.

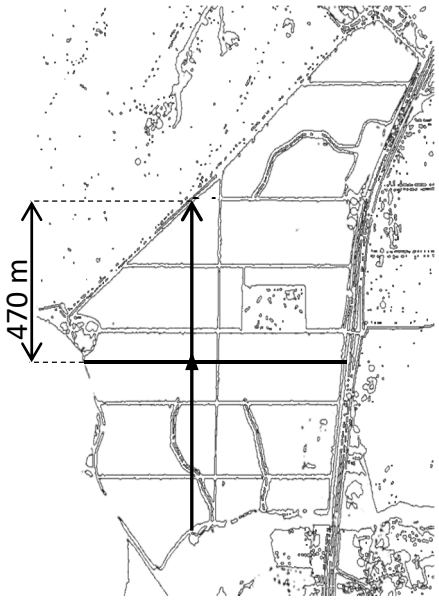

Figure 2. Olive orchard and location of the eddy covariance tower (black triangle, 38°24′46.3″N, 7°43′39.8″W).

The footprint analysis [56], performed to access the representativeness of the EC measurements, showed that over 90% of the fluxes sensed, determined as cumulative normalized flux (CNF), came from the region of interest, regarding the four main cardinal points. The fetch (distance to the edge of the plot) in the main directions, varying approximately between 350 and 500 m, was then considered adequate (Figure 3). Measurements were mainly affected by fluxes coming from an upwind area at a distance of 15 m from the tower (maximum of the one-dimensional footprint function, which provides the relative contribution to the vertical flux: $Q_f = (1/Q_o)\, dQ/dx$, for a given height z, being Q_o the latent heat flux density measured at point x = (0, z)).

Measurements in days with prevailing winds from the North-East direction were discarded given the vicinity of a building approximately at 200 m in that direction. Prevailing winds, calculated as average frequency for each of the EC measurement periods, were in agreement with historical climatic data, which indicates the North-West direction (Figure 4). Wind direction frequency was further analysed in detail for individual days and EC data screened accordingly for specific modelling purposes.

The energy balance equation closure error (Figure 5) was determined with a linear regression analysis forced to the origin using daily values of the measured fluxes (LE, H, R_n and G). The error, below 10% ($H + LE = 0.91\ (R_n - G)$, $R^2 = 0.87$), is similar to that found by other authors using this technique in orchards [57–59].

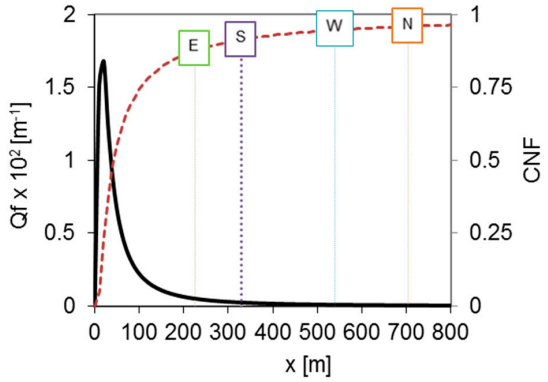

Direction	Fetch (m)	CNF
East	504	0.96
West	353	0.94
North	470	0.95
South	455	0.95

Figure 3. Cumulative normalized flux (CNF, dashed line) and relative contribution to the vertical flux for a given height z, (Q_f, continuous line) according to distance from the measurement point (EC tower) to the plot limit (x), obtained with footprint analysis; marked values for the fetch and CNF according to the cardinal directions; x is the distance between the observation point and the fluxes source region.

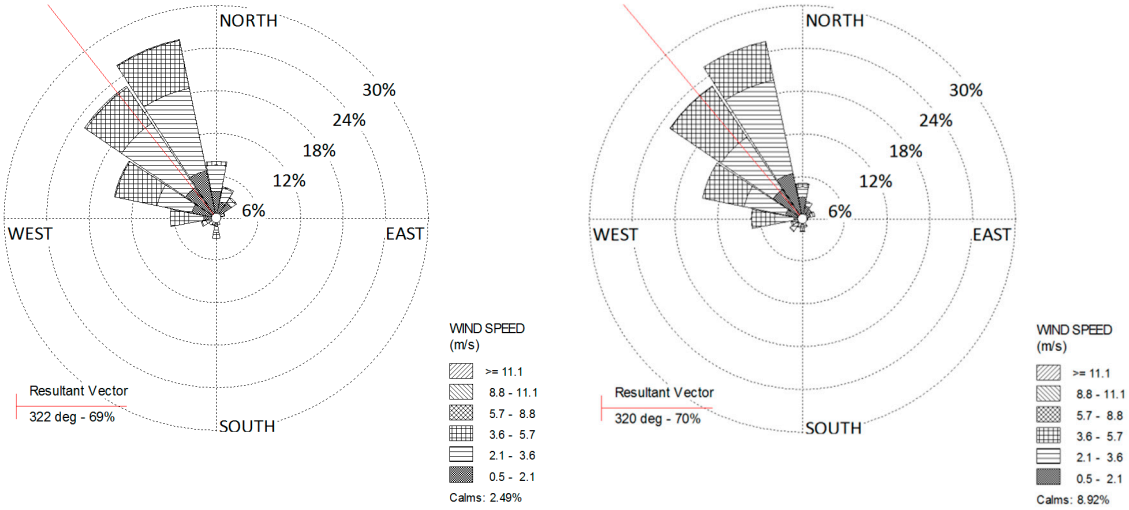

(**a**) (**b**)

Figure 4. Wind prevailing directions during periods of eddy covariance measurements and resultant vector, (**a**) July–August 2011, (**b**) June–August 2012 (deg.: degrees).

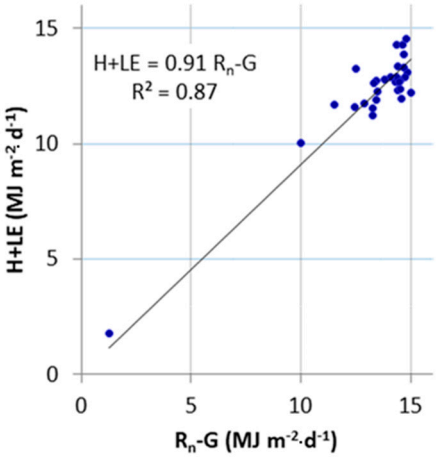

Figure 5. Surface energy balance equation for flux density daily values of LE (latent heat flux density), H (sensible heat flux density), G (soil heat flux density) and R_n (net radiation).

2.3. Transpiration from Sap Flow Measurements with the Granier Method

Plant transpiration was measured with thermal dissipation Granier probes [60] between DOY (day of year) 134 in 2011 and DOY 194 in 2013 (continuous half-hourly records). Six trees, chosen according to trunk diameter class frequency determined in a large sample of the orchard, were equipped with 1 cm length sensors (UP GmbH, Cottbus, Germany). Average data were stored each thirty minutes in a datalogger (Model CR1000, Campbell Scientific, Inc., Logan, UT, USA). Natural temperature gradients in the tree trunk were accounted for using data from non-heated sap flow sensors calculated during long periods. Daily transpiration was calculated from the half-hourly data. For flux calculation, the sapwood area in the cross section of the trunk was evaluated from core samples taken with an increment borer. Observation of the samples allowed considering the whole area conductive except the bark.

Sap flow methods are often referred as underestimating transpiration [19,61–65]. Although the original calibration of this method, which allows converting temperature differences between the two probes into crop transpiration, was initially considered universal, more recently, evidences show that it is advisable to verify its accuracy. Raw sap flow observations (SF, $mm \cdot d^{-1}$) were therefore corrected to obtain calibrated sap-flow transpiration (T_{SF}, $mm \cdot d^{-1}$), as referred in previous applications to tree crops [38,47,61]. This was done by mathematically relating sap-flow, SF, with transpiration computed from EC observations ($T_{EC} = ET_{EC} – E_{sim}$). T_{EC} represents the difference between ET obtained from EC measurements (ET_{EC}, $mm \cdot d^{-1}$) and the soil evaporation (E_{sim}, $mm \cdot d^{-1}$) simulated with the two phases Ritchie model [66], the latter computed following Allen et al. [4]. The computation of E_{sim} based upon the water balance of the soil evaporation layer using soil moisture observations. Parameters characterizing that soil layer, with a depth Z_e = 0.10 m, consisted of: total and readily evaporable water, respectively TEW = 18 mm and REW = 9 mm. Further information on E_{sim} data was provided by Paço et al. [19]. This procedure allows enlarging the available field information to the entire simulation period [67,68].

The best mathematical relationships between T_{EC} and SF (Figure 6) were of exponential form:

$$T_{EC} = K_{SF}\, e^{\alpha \cdot SF} \quad (2)$$

with K_{SF} = 0.34 and α = 1.40 (R^2 = 0.55; n = 13) for 2011 and K_{SF} = 0.34 and α = 1.72 (R^2 = 0.61; n = 28) for 2012, which was extended for 2013. The adjustment of SF was performed with Equation 2 assuming that the transpiration derived from sap-flow measurements (T_{SF}) equals that estimated from EC observations as referred above (T_{EC}). The approach used may be affected by uncertainties in computing E_{sim} as well as measurements errors affecting both T_{EC} and SF. Nevertheless, The T_{SF} values resulting from the application of Equation 2, which varied between 0.36 and 3.54 $mm \cdot d^{-1}$, are comparable to transpiration values reported for other studies on olive orchards [18,59,69].

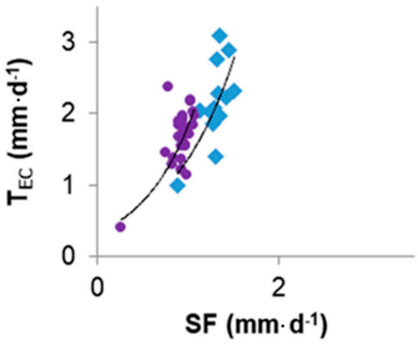

Figure 6. Relationships between the raw transpiration flux observed with the Granier sap-flow method (SF) and the transpiration rate computed from the eddy covariance observations (T_{EC}) relative to 2011 (squares) and 2012 (circles).

T_{SF} data were screened for outliers taking into consideration: (a) the range of values used to establish the sap flow calibration equation and the respective K_{cb} values ($K_{cb\,SF} = T_{SF}/ET_o$), which should be kept within an acceptable range. The common definition of outliers by Tukey [70] was used, thus considering as outliers the $K_{cb\,SF}$ values higher than 1.5 times the interquartile range, below the first quartile or above the third quartile. The application of these rules led to discarding a total of 177 T_{SF} values, with outliers representing 3.5% and 7% of observations in 2011 and 2012, respectively, contrasting with 56% of values computed for 2013. That high number of discarded values was most likely due to the fact that the SF equation used for 2013 was not purposefully calibrated. It was assumed that discarding the outliers decreased the uncertainties of observations and computations.

2.4. Basal Crop Coefficients Derived from Crop Height and Fraction of Ground Cover

To take into account fraction of ground cover by the crop (f_c) and the crop height (h), a density coefficient (K_d) is used with the A&P approach to estimate K_{cb} [43]. K_d (dimensionless) is defined as the minimum value among the effective ground cover corrected for the density of shading or corrected for the crop shading depending upon the crop height. Thus, K_d is given by:

$$K_d = \min(1, M_L\, f_{c\,eff}, f_{c\,eff}^{(1/(1+h))}) \quad (3)$$

where $f_{c\,eff}$ is the effective fraction of ground covered or shaded by vegetation near solar noon (dimensionless), M_L is a multiplier on $f_{c\,eff}$ describing the effect of canopy density on shading the ground, thus on maximum relative ET per fraction of ground shaded and h (m) is the mean height of the crop vegetation.

K_{cb} is estimated from K_d as

$$K_{cb} = K_{c\,min} + K_d\,(K_{cb\,full} - K_{c\,min}) \quad (4a)$$

when the inter-row is bare soil or, when an active ground cover is present, as

$$K_{cb} = K_{cb\,cover} + K_d\left(\max\left[K_{cb\,full} - K_{cb\,cover}, \frac{K_{cb\,full} - K_{cb\,cover}}{2}\right]\right) \quad (4b)$$

where $K_{c\,min}$ is the minimum K_c for bare soil (≈ 0.15 for typical agricultural conditions), $K_{cb\,cover}$ is the K_{cb} of the ground cover in the absence of tree foliage and reflects the density and vigour of the active ground cover crop and $K_{cb\,full}$ is the estimated basal K_{cb} during the peak plant growth for conditions having nearly full ground cover. The second term of the max function allows taking into consideration the impacts of shading of the canopy over the ground cover crop. Further information is provided by Allen and Pereira [43].

The $K_{cb\,full}$ represents a general upper limit on $K_{cb\,mid}$ for tall vegetation having full ground cover and LAI > 3 under full water supply. $K_{cb\,full}$ takes into consideration crop stomatal control and is approximated as a function of the mean plant height and adjusted for climate [43],

$$K_{cb\,full} = F_r\left(\min(1.0 + 0.1h,\ 1.20) + [0.04(u_2 - 2) - 0.004(RH_{min} - 45)]\left(\frac{h}{3}\right)^{0.3}\right) \quad (5)$$

with F_r (0–1) is an adjustment factor relative to crop stomatal control, the min function assumes that 1.20 is the upper bound for $K_{cb\,full}$ prior to adjustment for climate. h (m) is the average maximum crop height, u_2 (m s^{-1}) is the average wind speed at 2 m height, RH_{min} (%) is the average minimum relative humidity during mid-season.

The parameter F_r applies a downward adjustment when the vegetation exhibits more stomatal control on transpiration than it is typical of most annual agricultural crops. $F_r < 1.0$ for various tree crops and natural vegetation. Standard values for F_r for various tree crops are provided by Allen and Pereira [43] but F_r values may be adjusted experimentally, namely through comparing K_{cb} obtained

with the A&P approach with those derived through a different but accurate procedure, namely through the use of models. F_r may also be computed through comparing the leaf resistances for the crop (r_l, s m^{-1}) with that of grass (100 s m^{-1}) considering the climate conditions [43], thus:

$$F_r \approx \frac{\Delta + \gamma\,(1 + 0.34\,u_2)}{\Delta + \gamma\left(1 + 0.34\,u_2\,\frac{r_l}{100}\right)} \quad (6)$$

where r_l (s·m^{-1}) is mean leaf resistance for the vegetation in question (s·m^{-1}) Δ is the slope of the saturation vapour pressure curve (kPa·°C^{-1}), γ is the psychometric constant (kPa·°C^{-1}) and u_2 is the average wind speed during the relevant crop stage measured at 2 m height (m·s^{-1}). r_l values for various crops are tabulated by Allen e Pereira [43], who also referred that for most annual agricultural crops r_l is often not far from 100 s·m^{-1}.

2.5. The SIMDualKc Model

The SIMDualKc water balance model [34] uses a daily time step to perform the soil water balance at the field scale through computing crop ET with the dual K_c approach [4,33,43]. The SIMDualKc model adopts the approach described with Equation 1, thus assuming that $ET_{c\,act} = ET_c$ when the soil water depletion fraction does not exceeds the depletion fraction for no stress, p (dimensionless).

The model computes the soil water depletion at the end of every day:

$$D_{r,\,i} = D_{r,\,i-1} - (P_e - RO)_i - I_i - CR_i + ET_{cact,\,i} + DP_i \quad (7)$$

where $D_{r,i}$ and $D_{r,i-1}$ are the root zone depletion at the end of respectively day i and day i−1 (mm), P_e is precipitation (mm), RO is runoff (mm), I is the net irrigation depth that infiltrates the soil (mm), CR is capillary rise from the groundwater table (mm), $ET_{c\,act}$ is actual crop evapotranspiration (mm) and DP is deep percolation through the bottom of the root zone (mm), all referring to day i. CR and DP are calculated with parametric equations described by Liu et al. [71] and RO is estimated using the curve number approach [72]. Because the groundwater table is quite deep in the region, CR was assumed to be null.

The model computes the actual ET ($ET_{c\,act}$, mm) as a function of the available soil water in the root zone using a water stress coefficient (K_s, 0–1). K_s is computed daily as a linear function of the depletion D_r in the effective root zone [4,33]:

$$K_s = \frac{TAW - D_r}{TAW - RAW} = \frac{TAW - D_r}{(1-p)\,TAW} \rightarrow \text{for } D_r > RAW \quad (8)$$

$$K_s = 1 \rightarrow \text{for } D_r \leqslant RAW \quad (9)$$

where TAW and RAW are, respectively, the total and readily available soil water (mm) relative to the root zone depth Z_r and p is the soil water depletion fraction for no stress, therefore with RAW = p TAW. Thus, $ET_{c\,act} = ET_c$ when $K_s = 1.0$; otherwise, when water and/or salinity stress occurs, $ET_{c\,act} < ET_c$ and $K_s < 1.0$. Then, because $K_{cb\,act} = K_s\,K_{cb}$, it results $K_{cb\,act} < K_{cb}$. Similarly, it results that actual transpiration will be smaller than its potential value, thus $T_{c\,act} < ET_c$ when $K_s < 1.0$.

The evaporation from the soil surface (E_s, mm·d^{-1}) is limited by the amount of energy available at that surface in conjunction with the energy consumed as crop transpiration [4,72]. The model computes the evaporation coefficient (K_e) performing a daily water balance of the evaporation soil layer, which is characterized by its depth (Z_e, m), the total evaporable water (TEW, mm) and the readily evaporable water (REW, mm). TEW is the maximum depth of water that can be evaporated from the evaporation soil layer when that layer has been fully wetted and REW is the depth of water that can be evaporated without water availability restrictions. E_s is maximum when the topsoil is fully wetted by rain or irrigation and the soil surface shadowed by the crop is minimum. Differently, E_s is minimum when the crop fully shadows the soil and energy available for evaporation is minimum [4,34,72].

The maximum value of K_e is attained when the soil is wet. That value is limited by the energy available at the soil surface, which corresponds to the difference between $K_{c\,max}$, representing maximum ET when the crop would fully cover the soil and K_{cb}, representing the effective transpiration of the crop. As the topsoil dries, less water is available for evaporation and E_s is reduced. This reduction in E_s is proportional to the amount of water remaining in the surface soil layer. K_e is then computed considering an evaporation reduction coefficient ($K_r \leqslant 1.0$) as

$$K_e = K_r\,(K_{cmax} - K_{cb}) \rightarrow \text{with } K_e \leqslant f_{ew}\,Kc_{max} \tag{50}$$

where $K_{c\,max}$ is the maximum value of K_c (i.e., $K_{cb} + K_e$) following a wetting event by rain or irrigation, generally 1.20 and f_{ew} is the fraction of the soil that is both exposed to radiation and wetted by rain or irrigation, that is, the fraction of soil surface from which most evaporation occurs. Thus, f_{ew} depends upon the fraction of ground covered by the crop (f_c) and of the fraction of soil wetted by irrigation (f_w), thus $f_{ew} = \min(1-f_c, f_w)$. K_r is calculated using the 2-stage drying cycle approach [4,66], where the first stage is the energy limiting stage and the second is the water limited stage or falling rate stage, where evaporation decreases as evaporable water decreases in the evaporation soil layer beyond the readily evaporable water (REW):

$$K_r = 1 \rightarrow \text{for } D_{e,i-1} \leqslant REW \tag{61}$$

$$K_r = \frac{TEW - D_{e,\,i-1}}{TEW - REW} \text{ for } D_{e,i-1} > REW \tag{72}$$

Further descriptions of the model and auxiliary equations are given by Rosa et al. [34].

The input data required by the model include:

i Daily climatic data: reference evapotranspiration (ET_o, mm), precipitation (P, mm), minimum relative humidity (RH_{min}, %) and wind speed at 2 m height (u_2, $m{\cdot}s^{-1}$).

ii Soil data for a multi-layered soil: number of layers and related depths d (m); the respective soil water content at field capacity and at the wilting point (θ_{FC} and θ_{WP}, $m^3{\cdot}m^{-3}$) or the total available water (TAW, mm); the characteristics of the soil evaporation layer (Z_e, REW and TEW); and the soil water content at planting in both the root zone and the evaporation layer expressed as a % of depletion of TAW and TEW, respectively.

iii Crop data: dates of the crop growth stages (non-growing, initial, crop development, mid-season and end season); the basal crop coefficients for the non-growing, initial, mid-season and end season ($K_{cb\ non\text{-}growing}$, $K_{cb\ ini}$, $K_{cb\ mid}$ and $K_{cb\ end}$); the soil water depletion fractions for no stress at the same stages ($p_{non\text{-}growing}$, p_{ini}, p_{mid} and p_{end}); root depths (Z_r, m), plant height (h, m) and the fraction of ground cover by the crop (f_c, %) throughout the crop season.

iv Irrigation scheduling data: dates and depths of observed irrigation events. In addition, the model requires data relative to the fraction of soil wetted by irrigation (f_w). In this application, $f_w = 0.23$ because the soil was wetted by micro-irrigation.

v Parameters required to compute capillary rise and deep percolation when using the parametric equations proposed by Liu et al [71]; in the present application only the parameters a_D and b_D characterizing DP were used.

vi Base data to compute surface runoff using the Curve Number method [72].

vii Information characterizing the active ground cover, soil residues and mulches and related effects on E_s [34].

viii soil and water salinity information, however not used in the present application.

2.6. Model Calibration and Validation and Goodness of Fit Indicators

So far, the calibration and validation of the SIMDualKc model have been performed either through comparing computed actual transpiration with sap-flow measurements [38,39], simulated $ET_{c\,act}$ with

EC observed evapotranspiration [73,74] or, more commonly, simulated with observed soil water content [35,37,41,75,76]. In this study, model calibration was considered as the process of adjusting influential model parameters and inputs within their reasonable ranges so that the simulated $T_{c\ act}$ values were in agreement with sap flow derived data (T_{SF}).

The calibration procedure consisted of adjusting the crop parameters—K_{cb} and p values relative to the non-growing, initial-, mid- and end-season growth stages-, the soil evaporation parameters—TEW, REW and Z_e-, the deep percolation parameters a_D and b_D and the CN of the runoff curve number algorithm, by minimizing the differences between T_{SF} and simulated $T_{c\ act}$. Daily data of 2011 was used. An initial set of parameters was selected: crop parameters (K_{cb} and p) from Allen et al. [4] and Paço et al [19]; soil evaporation parameters from Paço et al. [19], CN from Allen et al. [72] and DP parameters from Paço et al. [19]. The initial soil water conditions in 2011 were observed in the field and consisted of the initial depletion of the evaporation layer, that was 40% of TEW and the initial depletion in the entire root zone, that was 40% of TAW. A trial and error procedure was then developed for selecting first the K_{cb} values. In the following, the trial and error procedure was applied to the p values, then to the referred soil evaporation, deep percolation and, lastly, to the CN parameters.

The validation of SIMDualKc consisted of using the previously calibrated parameters ($K_{cb\ non\text{-}growing}$, $K_{cb\ ini}$, $K_{cb\ mid}$, $K_{cb\ end}$, $p_{\ non\text{-}growing}$, $p_{\ ini}$, $p_{\ mid}$, $p_{\ end}$, TEW, REW, Z_e, a_D, b_D and CN) with daily data of 2012. T_{SF} data relative to 2013 was used for model testing with the same calibrated parameters. The process of calibration and validation was considered satisfactory when the goodness-of-fit indicators relative to the validation were within 20% of variation relative to the calibration.

A set of goodness-of-fit indicators were used to assess the model accuracy, as in prior studies with SIMDualKc. These indicators are fully described by Pereira et al. [37]. They included a linear regression coefficient (b_0) of the regression forced through the origin between observed T_{SF} and predicted $T_{c\ act}$ and the determination coefficient R^2 of the ordinary least squares regression. A regression coefficient b_0 close to 1.0 indicates that the predicted values are statistically close to the observed ones and a determination coefficient R^2 near 1.0 indicates that most of the variance of the observed values is explained by the model estimates. Errors of estimation were assessed using the root mean square error (RMSE) and the average absolute error (AAE) as indicators. Targeted values for error indicators are 0.0 which corresponds to a perfect match between simulated and observed values. In addition, to assess any bias tendency of the estimations, the percent bias (PBIAS, %) was used. The PBIAS measures the average tendency of predictions to be larger or smaller than the corresponding observations, with positive values indicating an over-estimation bias and negative values indicating an under-estimation bias. To assess the modelling quality, the Nash and Sutcliff [77] modelling efficiency (EF, dimensionless) was used. The EF is a normalized statistic that determines the relative magnitude of the residual variance compared to the measured data variance or how well observations versus simulations fit the 1:1 line [78]. EF values close to 1.0 indicate that the variance of residuals is much smaller than the variance of observations, thus that model performance is excellent. Contrarily, when EF is negative this means that there is no gain in using the model, thus that the mean of observations is as good predictor as the model.

3. Results and Discussion

3.1. Calibration and Validation of SIMDualKc with Sap Flow Data

The initial and calibrated values of the parameters relative to the SIMDualKc model are presented in Table 2 and they refer to the conditions observed in field. The calibrated K_{cb} parameters are smaller than the initial ones, mainly those relative to the non-growing season and the initial periods ($K_{cb\ non\text{-}growing}$ and $K_{cb\ ini}$). Differences for $K_{cb\ mid}$ resulted relatively small. However, $K_{cb\ mid}$ adjusted to the climate are slightly smaller than reported in Table 2 (0.44 to 0.47) because local climate is dry and RH_{min} is small, while $K_{cb\ end}$ are slightly increased (0.44 to 0.48) since RH_{min} is also increased

by the end-season. The calibrated p parameters closely follow those proposed by FAO56 [4]. Runoff CN changed little and deep percolation parameters did not change because these parameters were adjusted in a previous study [19].

Table 2. Initial and calibrated parameters used in SIMDualKc model.

Parameters		Initial	Calibrated
Crop	$K_{cb\ non\text{-}growing}$	0.50	0.30
	$K_{cb\ ini}$	0.50	0.30
	$K_{cb\ mid}$	0.55	0.48
	$K_{cb\ end}$	0.50	0.43
	$p_{non\text{-}growing}$	0.65	0.65
	p_{ini}	0.65	0.65
	p_{mid}	0.65	0.60
	p_{end}	0.65	0.65
Soil evaporation	TEW	18	18
	REW	9	9
	Z_e	0.10	0.10
Runoff	CN	72	75
Deep percolation	a_D	246	246
	b_D	−0.02	−0.02

$K_{cb\ non\text{-}growing}$—basal crop coefficient for the non-growing stage; $K_{cb\ ini}$—basal crop coefficient for the initial crop development stage, $K_{cb\ mid}$—basal crop coefficient for the mid stage, $K_{cb\ end}$—basal crop coefficient for the late-season stage, p—depletion fraction, M_L parameter, TEW—total evaporable water, REW—readily evaporable water, Z_e—thickness of the evaporation layer, CN—curve number, a_D and b_D—deep percolation parameters.

Most studies in literature report on actual K_{cb} values, that is, when the crop was affected by water stress since deficit irrigation is mostly used in olive orchards. In addition, most studies focus on the irrigation season only and data relative to other crop growth stages are quite scarce, namely for the non-growing period and initial crop stage. Moreover, K_{cb} values reported in literature are not adjusted to the climate. Therefore, it results difficult to compare our results with those relative to other studies. $K_{cb\ mid}$ values of this study are similar to those reported by Santos et al. [26] when using remote sensing observations of an olive orchard under water stress conditions. Slightly lower $K_{cb\ mid}$ values were reported by Conceição et al. [59]. Differently, López-Olivari et al [69] reported much lower $K_{cb\ mid}$ values, averaging 0.28, which is likely due to water stress as commonly imposed by farmers. Higher $K_{cb\ mid}$ values (0.58 ± 0.14) were reported by Cammalleri et al. [18] for an intensive olive orchard with $f_c = 0.35$. Er-Raki et al. [20] also reported a higher $K_{cb\ mid}$ of 0.54. Much higher K_{cb} values were proposed by Allen and Pereira [43]. The p values are similar to those reported by Er-Raki et al. [20] and by Rallo et al. [79].

Results in Figure 7, comparing model simulated $T_{c\ act}$ with transpiration derived from sap-flow measurements (T_{SF}), show a good agreement between $T_{c\ act}$ and T_{SF} along the three years of study. The dynamics of both $T_{c\ act}$ and T_{SF} are coherently described for all three years but fitting is less good for 2012 due to the heavy frost and subsequent pruning that occurred by that winter. Apparently, the trees responded well to pruning and that exceptional condition could have justified using specific K_{cb} and p values but that option was not adopted because validating the model requires using the calibrated parameters. However, despite the peculiar condition occurring in 2012, as well as the uncertainties associated with deriving T_{SF}, model predicted $T_{c\ act}$ described reasonably well the dynamics of transpiration of the olive orchard throughout the three experimental seasons.

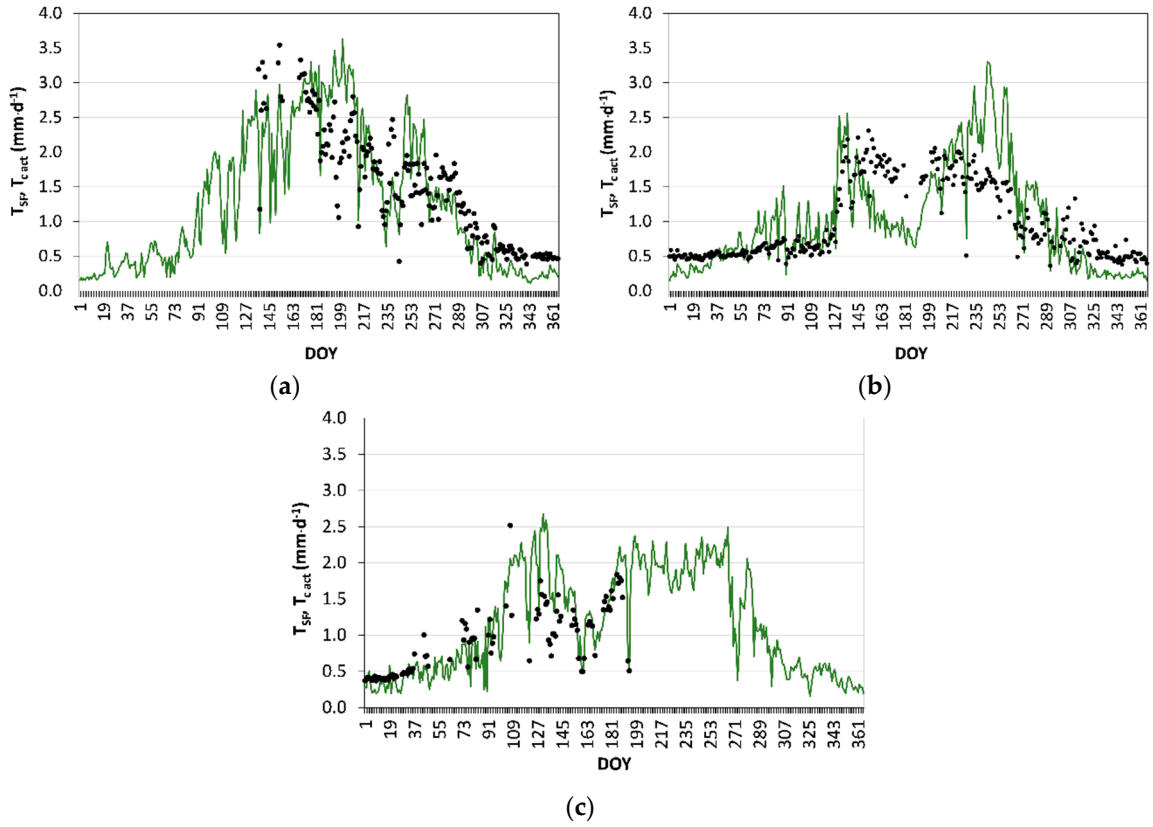

Figure 7. Simulated transpiration dynamics ($T_{c\,act}$, —) compared with sap flow adjusted transpiration (T_{SF}, •) in the (**a**) calibration (2011), (**b**) validation (2012) and (**c**) testing (2013).

The goodness-of-fit indicators (Table 3) show a slight tendency for the model to over-estimate T_{SF}, with b_0 = 1.04 and PBIAS = 3.9% in the calibration year; the same trend for over-estimation was observed in 2012 and 2013, with b_0 of 1.03 and 1.17 and PBIAS of 5.2% and 13.3%. The determination coefficients are high for the first and third years, with respectively R^2 = 0.75 and 0.78; due to the problems identified to 2012, it resulted R^2 = 0.60, however reasonably high. These R^2 values indicate, therefore, that a large fraction of the variance of T_{SF} is explained by the model. Estimation errors are reasonably low, with RMSE ranging from 0.37 to 0.53 mm·d^{-1} and AAE ranging from 0.25 to 0.42 mm·d^{-1}. The modelling efficiency is reasonably high for the calibration year, with EF = 0.57 and acceptable for the validation and testing years. Overall, results for the goodness-of-fit indicators show that the predicted $T_{c\,act}$ values were statistically close to the sap-flow observed ones and that most of the variation of the observed values is explained by the model. Higher errors of estimation were reported by Rallo et al. [79] when using a modification of the FAO56 approach for an intensive olive orchard, with RMSE ranging from 0.30 to 0.78 mm·d^{-1}. Er-Raki et al. [20], also reported higher $T_{c\,act}$ estimation errors, with RMSE = 0.59 mm·d^{-1}.

Table 3. Goodness-of-fit indicators relative to the SIMDualKc simulated transpiration ($T_{c\,act}$) when compared with transpiration obtained from sap flow (T_{SF}).

	n	b_0	R^2	PBIAS (%)	RMSE (mm·d^{-1})	AAE (mm·d^{-1})	EF
Calibration, 2011	201	1.04	0.75	2.0	0.53	0.42	0.57
Validation, 2012	338	1.04	0.60	3.0	0.47	0.36	0.25
Testing, 2013	111	1.17	0.78	13.3	0.37	0.25	0.35

n = number of observations, b_0 = regression coefficient, R^2 = determination coefficient, PBIAS = percent bias; RMSE = root mean square error, ARE = average relative error, AAE = average absolute error, EF = modelling efficiency.

The dynamics of the actual crop evapotranspiration ($ET_{c\ act}$) simulated along 2011 and 2012, which was computed with the calibrated model parameters of Table 2, is presented in Figure 8. $ET_{c\ act}$ are compared with evapotranspiration values observed with the eddy covariance system (ET_{EC}). Despite ET_{EC} observations were in reduced number, they could be used for further validate the model since results show that the model was able to adequately estimate the dynamics of $ET_{c\ act}$ during the mid-season stage when ET_{EC} was measured. The average ET_{EC} value during this stage was 2.5 mm·d^{-1} ($\pm$0.41, n = 28). Goodness-of-fit indicators for 2012 show a tendency for the SIMDualKc model to under-estimate ET_{EC} (b_0 = 0.94 and PBIAS = −6.0%), thus contrary to the tendency observed when $T_{c\ act}$ was compared with T_{SF}. However, given the reduced number of EC observations, it is not possible to draw a conclusion about model trending. An acceptably high R^2 = 0.64 was obtained, which indicates that a large fraction of the variance of ET_{EC} observations is explained by the model. In addition, acceptable estimation errors of $ET_{c\ act}$ were obtained with RMSE = 0.42 mm·d^{-1}, AAE = 0.35 mm·d^{-1} and, consequently, a reasonably good EF value of 0.45 was obtained. Higher estimation errors for $ET_{c\ act}$, ranging from 0.54 to 0.71 mm·d^{-1}, were reported by Er-Raki et al. [20].

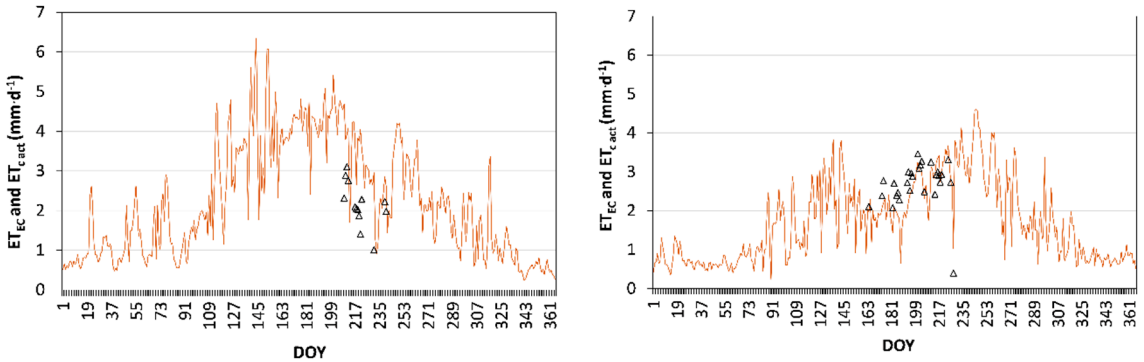

Figure 8. Actual crop evapotranspiration dynamics measured with Eddy covariance (ET_{EC}, Δ) and simulated with SIMDualKc ($ET_{c\ act}$, —) for (**a**) 2011 and (**b**) 2012.

3.2. Dual and Single Crop Coefficients

The standard and actual K_{cb} curves, the K_e curves and the standard and actual single K_c curves derived for the 3-year observed hedgerow olive orchard are shown in Figure 9. Precipitation and irrigation events are also depicted to easily interpreting the behaviour of the K_e, K_{cb} and K_c curves. The represented K_{cb} values were adjusted for climate as a function of wind speed, RH_{min} and crop height as proposed in FAO56 [4], so resulting slightly different from those given in Table 2 as referred before. The time-averaged standard K_c relative to the various crop stages was computed by summing the standard K_{cb} of the same crop stages with the daily K_e values computed for the same periods, that is, $K_c = K_{cb} + K_e$. Differently, $K_{c\ act} = K_{cb\ act} + K_e$, thus varying daily.

The K_{cb} and $K_{cb\ act}$ curves (Figure 9) are coincident during winter and most of autumn and spring periods when rainfall was enough to avoid water stress, that is, when $K_{cb\ act} = K_{cb}$ as discussed about Equation 1. Differently, high water stress occurred during most of the mid-season stage, particularly during 2012 and 2013, when those curves indicated $K_{cb\ act} < K_{cb}$. This water stress occurred because the orchard was under-irrigated following the common practice of deficit irrigation in olive orchards, in particular because irrigations were started too late in those years. To achieve a eustress irrigation management it would be desirable that irrigation would start earlier in both 2012 and 2013, eventually adopting larger irrigation depths applied every two or three days instead of 3 mm depths every day. However, further studies are required to better defining the best eustress management with consideration of impacts of transpiration deficits on yields.

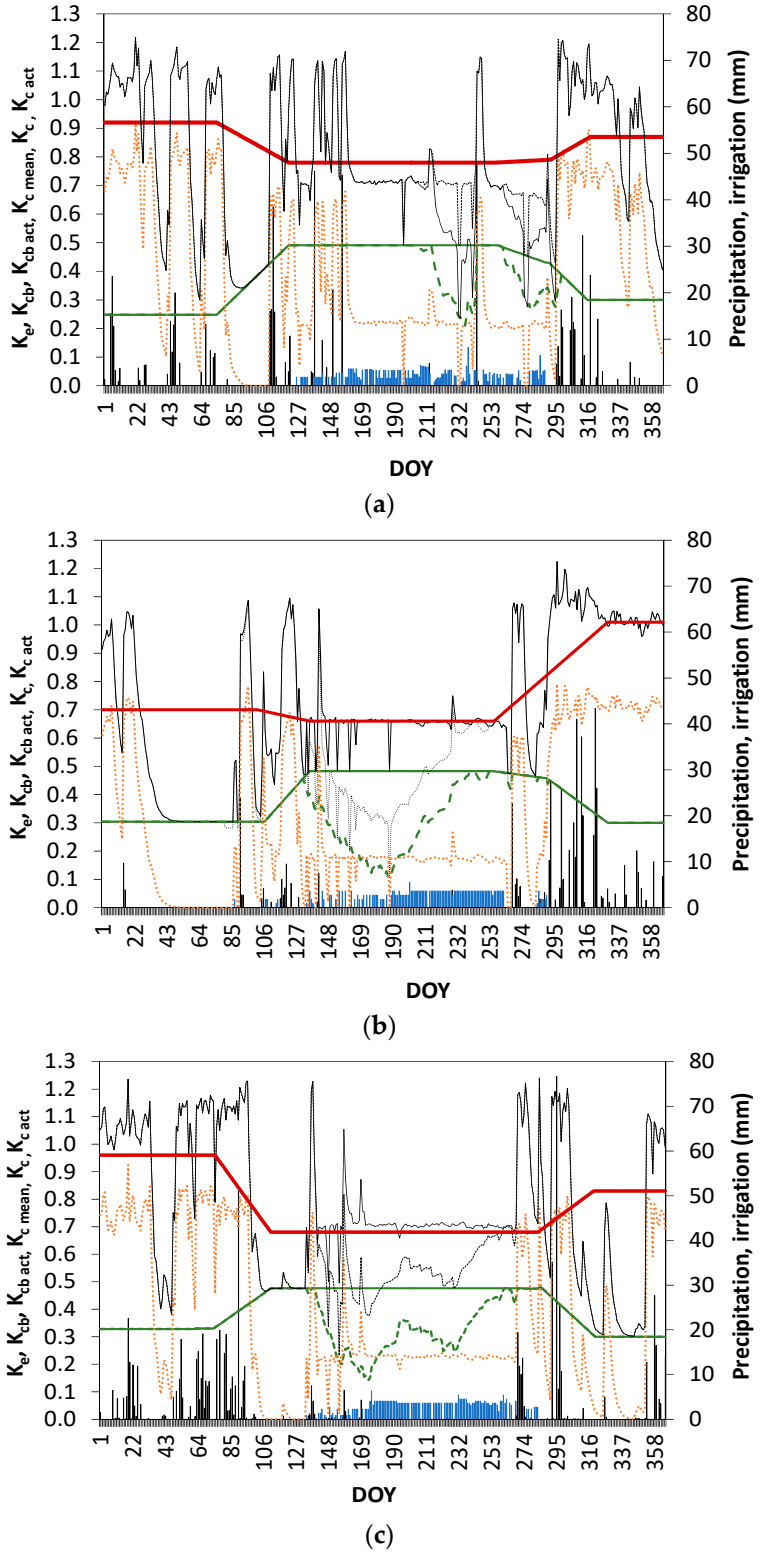

Figure 9. Standard and actual basal crop coefficients (K_{cb}, $K_{cb\ act}$), evaporation coefficient (K_e) and standard and actual single crop coefficients (K_c, $K_{c\ act}$) for a super-intensive olive orchard for: (**a**) 2011, (**b**) 2012 and (**c**) 2013, with depicting precipitation and irrigation events. K_{cb} (—) $K_{cb\ act}$ (- - -) K_e (. . .) $K_{c\ mean}$ (—) K_c (—) $K_{c\ act}$ (. . .) precipitation (I), irrigation (I).

Soil evaporation K_e curves show to react daily to the soil wetting events, mainly with various peaks occurring in response to rainfall events (Figure 9). During the rainfall season, from early autumn

to early spring, K_e is often high because the inter-row is wide and solar energy is then available at the soil surface. During mid-season soil evaporation decreases and K_e drops because soil dries and residues of the ground cover vegetation act as an organic mulch to limit evaporation. K_e peaks are much small during most of the mid-season stage because irrigation was applied along the row of trees, so under crop shadow, thus resulting in limited energy available for evaporating the irrigation water.

Differently of the time-averaged standard K_c curves, the $K_{c\ act}$ curves show numerous peaks in response to the rainfall events (Figure 9) since these curves represent $K_{c\ act} = K_{cb\ act} + K_e$ as referred above. The K_c and $K_{c\ act}$ curves are coincident in the periods without water stress, thus during the rainy season, roughly from October to May. The standard and actual K_c values during the non-growing periods and the initial stage are highly dependent upon the precipitation amounts. Differently, the $K_{c\ act}$ curves lay bellow the K_c curve under water stress conditions during mid-season.

Figure 9 clearly shows the contrasting behaviour of standard K_c and K_{cb}. The above described dynamics of K_c curves, particularly the dependence of K_c values from soil evaporation, mainly due to soil wettings by precipitation, explains why the time-averaged standard $K_{c\ mid}$ is smaller than $K_{c\ non\text{-}growing}$ and $K_{c\ ini}$, that refer to the rainy season, while the higher standard K_{cb} values are for the mid-season, $K_{cb\ mid}$, thus when transpiration is higher under irrigation.

The time averaged K_c are presented in Table 4 for all crop stages of 2011, 2012 and 2013. $K_{c\ ini}$ values, ranging 0.70 to 0.96, are in the range of values reported for intensive olive orchards [43,80,81]. The $K_{c\ mid}$ values ranged 0.70 to 0.78, which are comparable with values reported by various authors [18,43,81,82]. K_c values for the late season (0.79 to 0.90) increased relative to the mid-season due to the occurrence of various precipitation events. High $K_{c\ end}$ values found in the present study are comparable with those reported by Testi et al. [80].

Table 4. Time-averaged crop coefficients (K_c) for the different crop growth stages.

Crop Growth Stages	2011	2012	2013
Non-growing *	0.91	0.77	0.75
Initial	0.96	0.70	0.96
Crop development	0.96–0.78	0.70–0.66	0.96–0.68
Mid-season	0.78	0.66	0.68
Late season	0.78–0.79	0.66–0.90	0.68–0.83
End season	0.79	0.90	0.83

* average value relative to both non-growing periods, by the end and the beginning of the year.

3.3. K_{cb} Predicted with the A&P Approach vs. K_{cb} Obtained with SIMDualKc

The A&P approach (Section 2.4, Allen & Pereira [43]) was applied with f_c and h data observed along the three seasons. The dynamics of f_c and h are presented in Figure 10a in conjunction with the corresponding computed values for K_{cb} ($K_{cb\ A\&P}$), which are compared with the standard K_{cb} obtained with SIMDualKc for the same days ($K_{cb\ SIMDualKc}$), resulting a close match (Figure 10b) except for the cases that follow the heavy frost with great defoliation and severe pruning in the winter of 2012.

When computing the density coefficient K_d (Equation (3)) the value $M_L = 1.5$ proposed by Allen and Pereira [43] was used. Nevertheless, because insufficient information on shadowing was available, it was assumed $f_c = f_{c\ eff} \cdot K_{cb\ full}$ (Equation (5)) was computed with observed weather data for the various crop stages and considering the observed crop height. The F_r values were obtained after applying a simple trial and error procedure against the values obtained by the model. That trial and error procedure was initiated with the value $F_r = 0.48$ proposed by Allen and Pereira [43] for the entire season and olive orchards without ground cover but just with residues of old leaves. The resulting value for the non-growing and the initial stages was $F_r = 0.49$, thus about the same as the proposed one, while values for both the mid- and late-season were respectively 0.55 and 0.53. These slightly higher values of F_r were likely due to the fact that less stomatal control was required by Arbequina olives

under irrigation. Nevertheless, the estimated F_r = 0.48 proposed by Allen and Pereira [43] would also provide for quite good K_{cb} estimations.

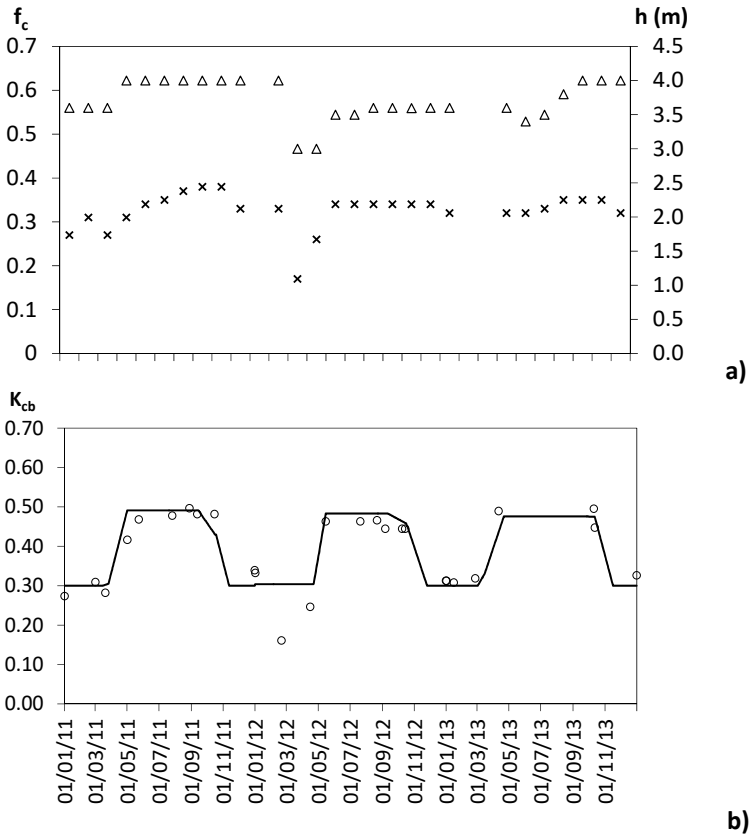

Figure 10. (**a**) Fraction of ground cover (f_c, x) measured and/or derived from SAVI and olives height (h, Δ) observed and (**b**) K_{cb} estimates using the A&P approach (○) compared with the K_{cb} curve computed with the SIMDualKc model (—) for the period 2011 to 2013.

For the period from November to April, K_{cb} were computed from K_d with Equation 4b relative to the case when active ground cover exists. A variable $K_{cb\ cover}$, from 0.004 to 0.01, was used. For May to October, the Equation 4a was used with $K_{c\ min}$ = 0.15

Results in Figure 10b show that K_{cb} computed with the A&P approach match quite well the $K_{cb\ SIMDualKc}$ except for the cases that follow the heavy frost that occurred in the winter of 2012, which produced a great defoliation and required a severe pruning. Consequently, $K_{cb\ A\&P}$ were then smaller than the $K_{cb\ non\text{-}growing}$ obtained with SIMDualKc. For all other cases, $K_{cb\ A\&P}$ values were close to the $K_{cb\ SIMDualKc}$ estimates.

The regression coefficient relating both K_{cb} sets (Figure 11) results close to the unit (b_0 = 0.97), thus indicating a good overall match, while the determination coefficient is high (R^2 = 0.77). The estimation of $K_{cb\ A\&P}$ approach has a small RMSE of 0.05 relative to the modelled $K_{cb\ SIMDualKc}$ values. Comparing the mean square error of $K_{cb\ A\&P}$ with the variance of the $K_{cb\ SIMDualKc}$ values it resulted a high EF of 0.76. In conclusion, results of comparing both sets of K_{cb} values indicate that the A&P approach is adequate for estimating K_{cb} values to be used when assessing crop water requirements for olives and to support irrigation management decision making.

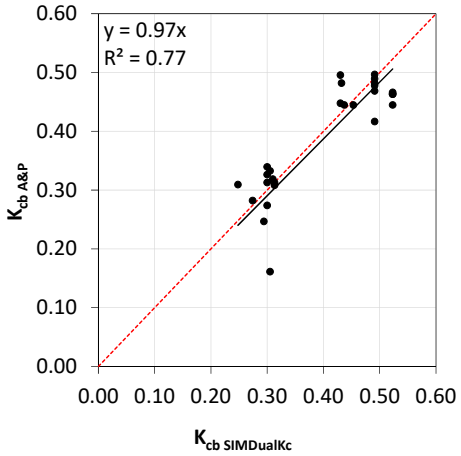

Figure 11. Linear regression forced to the origin of the K_{cb} values estimated with the A&P approach compared with the K_{cb} values obtained from the SIMDualKc model; also depicted the 1:1 line (- - -).

3.4. Water Balance and Respective Components

The terms of the soil water balance computed with the SIMDualKc model are presented in Table 5. There are appreciable differences among years which mainly steam from the differences in precipitation (P, mm). This is particularly the case of deep percolation and runoff (DP and RO, mm), which are much higher in the wet year of 2013, representing 47% of precipitation, which contrast with smaller DP and RO values in 2011 that represent 34% of the precipitation total. Those percent values indicate that most of precipitation, 53 to 66%, was used by the crop. As it could be expected, the larger amount of DP and RO occurred during the non-growing, initial, crop development and late season crop stages, that is, during the rainy season, which coincides with the period when crop water demand, evapotranspiration, is smaller as analysed relative to Figures 7 and 9. However, the distribution of DP and RO throughout the year varied enormously as a consequence of the inter- and intra-annual variability of the precipitation, as it may be noticed in Figure 1. DP and RO were very small during the mid-season and their occurrence refers only to a few rainfall events. The use of small drip irrigation applied depths makes that DP and RO are not originated by irrigation; moreover, the deficit irrigation management adopted also, likely, did not influence DP or RO occurrences.

The soil water storage (ΔSW, mm) at end of each crop stage and of the year greatly varied inter and intra-annually, mostly due to the referred variability of precipitation and likely less influenced by irrigation management as indicated by similar ΔSW values at end of the late season. This fact agrees with the conclusion that the adopted deficit irrigation management did not contribute to operational water losses.

Because rainfall was very small during the periods of large crop water demand, irrigation represented 39%, 56% and 50% of $ET_{c\,act}$ respectively in 2011, 2012 and 2013. Overall, irrigation occurred during the mid- and late season, mainly the former. These results show the great contribution of irrigation to achieve successful olives growth and yields, particularly in case of super-intensive olives orchards. Naturally, most of evapotranspiration occurred during the mid-season and, however less important, during the late-season. Soil evaporation exceeded transpiration during the non-growing and initial crop stages because E_s mostly originated from the inter-row when wetted by rainfall. The large values of E_s estimated for the mid-season were mostly due to rainfall events that occurred early in that season; similarly, most of E_s estimated for the late season also were due to rainfall events wetting the exposed inter-row. E_s originated from irrigation was reduced because energy available under the canopy shadow was little.

Table 5. Simulated soil water balance components (all variables in mm).

Crop Growth Stages	Year	P	I	ΔSW	RO	DP	E_s	$T_{c\,act}$	$ET_{c\,act}$
Non-growing	2011	189	0	−20	11	54	70	34	104
	2012	76	0	35	0	30	37	45	82
	2013	224	0	−20	12	85	63	43	106
Initial	2011	37	0	−16	0	3	11	7	18
	2012	36	5	8	0	0	20	30	50
	2013	106	0	−15	5	54	23	10	33
Development	2011	95	0	15	18	11	27	54	81
	2012	33	4	14	0	0	21	30	51
	2013	159	0	40	31	89	38	41	79
Mid-season	2011	203	260	63	1	28	186	311	497
	2012	13	299	−4	0	0	117	191	308
	2013	29	358	54	0	0	173	269	442
Late season	2011	141	59	−77	10	2	48	63	111
	2012	353	42	−89	70	102	60	74	134
	2013	218	34	−58	27	45	55	62	117
Full year	2011	665	319	−35	40	98	342	469	811
	2012	511	350	−36	70	132	255	370	625
	2013	736	392	1	75	273	352	425	777

P = precipitation, I = net irrigation depths, ΔSW = variation in stored soil water, RO = runoff, DP = deep percolation, E_s = soil evaporation, $T_{c\,act}$ = actual crop transpiration, $ET_{c\,act}$ = actual crop evapotranspiration.

The consumptive use of water is analysed in Table 6. The ratios of $E_s/ET_{c\,act}$ show that E_s represents 45 to 67% of $ET_{c\,act}$ during the non-growing stage and 40 to 70% during the initial crop stage. These periods are those when more precipitation occurs, so where the soil is frequently wetted by rain and soil cover is less, particularly in the inter-row. Thus, soil evaporation is the main consumptive water use during those stages. During the crop development, mid-season and late season stages, transpiration becomes the most important, corresponding to 52 to 67% of $ET_{c\,act}$. The variability of the ratio $E_s/ET_{c\,act}$ is then quite small, depending upon the occurrence of precipitation, which is the main source of soil wetting in the inter-row and of the subsequent evaporation. E_s could likely be reduce if less frequent but larger irrigation amounts would be used instead of daily irrigation events averaging 3 mm per event. $E_s/ET_{c\,act}$ ratios smaller than those computed in this study were reported by various researchers but referring to the irrigation season only [18,20,69]. Less frequent irrigations are also referred in these studies.

Table 6. Ratios of soil evaporation to actual evapotranspiration ($E_s/ET_{c\,act}$, %) and of actual to potential evapotranspiration ($ET_{c\,act}/ET_c$ %).

	Years	Non-Growing Periods	Initial	Development	Mid-Season	Late-Season	Whole Year
$E_s/ET_{c\,act}$ (%)	2011	67	61	33	37	43	42
	2012	45	40	41	38	45	41
	2013	59	70	48	39	47	45
$ET_{c\,act}/ET_c$ (%)	2011	100	100	100	94	88	97
	2012	100	100	98	70	99	82
	2013	100	100	100	78	100	86

Results relative to the ratio $ET_{c\,act}/ET_c$ (Table 6) show that $ET_{c\,act}$ was smaller by 3%, 18% and 14% relative to the potential ET_c in 2011, 2012 and 2013, respectively. During the mid-season, that ratio $ET_{c\,act}/ET_c$ was small for the years of 2012 and 2013, when $ET_{c\,act}$ was smaller by respectively 30% and 22% comparatively to the potential ET_c. Those decreases are likely excessive as analysed before (Figure 9) and may have affected yields, namely that of 2012. Adopting eustress irrigation, the ratio

$ET_{c\ act}/ET_c$ should likely not decrease below 90%. However, this threshold needs to be better assessed in terms of yield and economic impacts.

4. Conclusions

The calibration, validation and testing of the SIMDualKc model for a super high density Arbequina olive orchard was successfully performed using measurements of sap flow plant transpiration and eddy covariance evapotranspiration. Three years of field studies, from 2011 to 2013, were used, which made it possible to partitioning olive orchard ET into actual transpiration and soil evaporation. The results showed a good accuracy of the model to simulate transpiration during both the growing and non-growing seasons. Goodness of fit indicators were less good for 2012 when the orchard suffered an intense defoliation following a great frost and, later, a heavy pruning. However, the model could well represent the dynamics of evapotranspiration, transpiration and soil evaporation throughout the three years.

The calibration of the model and its validation and testing provided for updated basal and single crop coefficient curves for potential and actual crop water use, as well as soil evaporation coefficients. The standard K_{cb} were close to 0.30 during the non-growing and initial crop stages and 0.48 during the mid-season. Differently, the standard K_c varied from 0.70 to 0.96 during the non-growing and initial crop stages and decreased to 0.66 to 0.78 during the mid-season. The variability of standard K_c values results from the fact that, contrarily to K_{cb}, the K_c values depend upon soil evaporation, consequently also upon precipitation. It may be concluded that for perennial crops, as olive orchards and other woody crops, it is important to focus on using the dual instead of single K_c, thus in using basal K_{cb}.

The A&P approach for estimating K_{cb} values from the fraction of ground cover and crop height was tested against the K_{cb} values obtained with the model SIMDualKc after calibration. The K_{cb} obtained with A&P matched well the K_{cb} values obtained from SIMDualKc. Thus, results allow assuming that the A&P approach is useful to accurately estimating the K_{cb} values required to assess crop water requirements and deciding irrigation management practices of olives orchards. Likely, that conclusion may be extended to other crops under condition of properly parameterizing $K_{cb\ full}$ used for computing K_{cb} from f_c and h.

For the three years, deep percolation and runoff totalized 34% to 47% of the precipitation, thus with most of precipitation being used as crop evapotranspiration. Those percent values highly depend upon the annual distribution of precipitation and were not depending upon irrigation because frequent and small application depths were used. Soil water storage also revealed to vary along the year with precipitation. Soil evaporation ranged from 42% to 45% of annual olives ET, with $E_s > T_{c\ act}$ during the rainy season, the contrary occurring during the irrigation period. This fact also relates with the above referred irrigation management practiced. Irrigation amounts for 39% to 56% of the actual crop ET, which confirms the great importance of irrigation for super intensive olive orchards. However, those amounts correspond to deficit irrigation, with $ET_{c\ act}$ smaller than potential ET_c by 30% and 22% in 2012 and 2013, respectively. Those deficits are apparently excessive relative to a desirable eustress management that could lead to high yields and save water. Further research is required along these lines.

Author Contributions: T.A.P. and L.S.P. conceptualization, T.A.P., P.P. and L.S.P. methodology, P.P. calibration and validation of the model, T.A.P., P.P., J.S. and L.S.P. formal data analysis, J.S. and F.L.S. resources, T.A.P. and P.P. original draft preparation, L.S.P. review and editing, F.L.S. project supervision.

Funding: This study was supported by the projects PTDC/AGR-PRO/111717/2009 and EXPL/AGR-PRO/1559/2012 and the research unit LEAF (UID/AGR/04129/2013) funded by "Fundação para a Ciência e a Tecnologia," Portugal. The second author also acknowledges the same institution for a Post-Doc research grant (SFRH/BPD/79767/2011).

Conflicts of Interest: The authors declare no conflict of interest.

References

1. Connor, D.J.; Gómez-del-Campo, M.; Rousseaux, M.C.; Searles, P.S. Structure, management and productivity of hedgerow olive orchards: A review. *Sci. Hortic.* **2014**, *169*, 71–93. [CrossRef]
2. Trentacoste, E.R.; Puertas, C.M.; Sadras, V.O. Effect of irrigation and tree density on vegetative growth, oil yield and water use efficiency in young olive orchard under arid conditions in Mendoza, Argentina. *Irrig. Sci.* **2015**, *33*, 429–440. [CrossRef]
3. Ahumada-Orellana, L.E.; Ortega-Farías, S.; Searles, P.S. Olive oil quality response to irrigation cut-off strategies in a super-high density orchard. *Agric. Water Manag.* **2018**, *202*, 81–88. [CrossRef]
4. Allen, R.G.; Pereira, L.S.; Raes, D.; Smith, M. *Crop Evapotranspiration Guidelines for Computing Crop Water Requirements*; FAO: Rome, Italy, 1998; p. 300.
5. Pereira, L.S.; Oweis, T.; Zairi, A. Irrigation management under water scarcity. *Agric. Water Manag.* **2002**, *57*, 175–206. [CrossRef]
6. Palese, A.M.; Nuzzo, V.; Favati, F.; Pietrafesa, A.; Celano, G.; Xiloyannisa, C. Effects of water deficit on the vegetative response, yield and oil quality of olive trees (*Olea europaea* L., cv Coratina) grown under intensive cultivation. *Sci. Hortic.* **2010**, *125*, 222–229. [CrossRef]
7. Rallo, G.; Provenzano, G. Modelling eco-physiological response of table olive trees (*Olea europaea* L.) to soil water deficit conditions. *Agric. Water Manag.* **2013**, *120*, 79–88. [CrossRef]
8. Fernández, J.E.; Perez-Martin, A.; Torres-Ruiz, J.M.; Cuevas, M.V.; Rodriguez-Dominguez, C.M.; Elsayed-Farag, S.; Morales-Sillero, A.; García, J.M.; Hernandez-Santana, V.; Diaz-Espejo, A. A regulated deficit irrigation strategy for hedgerow olive orchards with high plant density. *Plant Soil* **2013**, *372*, 279–295. [CrossRef]
9. Gómez-del-Campo, M. Summer deficit-irrigation strategies in a hedgerow olive orchard cv. 'Arbequina': Effect on fruit characteristics and yield. *Irrig. Sci.* **2013**, *31*, 259–269. [CrossRef]
10. Padilla-Díaz, C.M.; Rodriguez-Dominguez, C.M.; Hernandez-Santana, V.; Perez-Martin, A.; Fernández, J.E. Scheduling regulated deficit irrigation in a hedgerow olive orchard from leaf turgor pressure related measurements. *Agric. Water Manag.* **2016**, *164*, 28–37. [CrossRef]
11. Padilla-Díaz, C.M.; Rodriguez-Dominguez, C.M.; Hernandez-Santana, V.; Perez-Martin, A.; Fernandes, R.D.M.; Montero, A.; García, J.M.; Fernández, J.E. Water status, gas exchange and crop performance in a super high density olive orchard under deficit irrigation scheduled from leaf turgor measurements. *Agric. Water Manag.* **2018**, *202*, 241–252. [CrossRef]
12. Tanasijevic, L.; Todorovic, M.; Pizzigalli, C.; Lionello, P.; Pereira, L.S. Impacts of climate change on olive crop evapotranspiration and irrigation requirements in the Mediterranean region. *Agric. Water Manag.* **2014**, *144*, 54–68. [CrossRef]
13. Haworth, M.; Marino, G.; Brunetti, C.; Killi, D.; De Carlo, A.; Centritto, M. The Impact of Heat Stress and Water Deficit on the Photosynthetic and Stomatal Physiology of Olive (*Olea europaea* L.)—A Case Study of the 2017 HeatWave. *Plants* **2018**, *7*, 76. [CrossRef] [PubMed]
14. Allen, R.G.; Pereira, L.S.; Howell, T.A.; Jensen, M.E. Evapotranspiration information reporting: I. Factors governing measurement accuracy. *Agric. Water Manag.* **2011**, *98*, 899–920. [CrossRef]
15. Egea, G.; Diaz-Espejo, A.; Fernández, J.E. Soil moisture dynamics in a hedgerow olive orchard under well-watered and deficit irrigation regimes: Assessment, prediction and scenario analysis. *Agric. Water Manag.* **2016**, *164*, 197–211. [CrossRef]
16. Rallo, G.; Provenzano, G.; Castellini, M.; Puig-Sirera, A. Application of EMI and FDR sensors to assess the fraction of transpirable soil water over an olive grove. *Water* **2018**, *10*, 168. [CrossRef]
17. Ramos, A.F.; Santos, F.L. Water use, transpiration and crop coefficients for olives (cv. Cordovil), grown in orchards in Southern Portugal. *Biosyst. Eng.* **2009**, *102*, 321–333. [CrossRef]
18. Cammalleri, C.; Rallo, G.; Agnese, C.; Ciraolo, G.; Minacapilli, M.; Provenzano, G. Combined use of eddy covariance and sap flow techniques for partition of ET fluxes and water stress assessment in an irrigated olive orchard. *Agric. Water Manag.* **2013**, *120*, 89–97. [CrossRef]
19. Paço, T.A.; Pocas, I.; Cunha, M.; Silvestre, J.C.; Santos, F.L.; Paredes, P.; Pereira, L.S. Evapotranspiration and crop coefficients for a super intensive olive orchard. An application of SIMDualKc and METRIC models using ground and satellite observations. *J. Hydrol.* **2014**, *519*, 2067–2080. [CrossRef]

20. Er-Raki, S.; Chehbouni, A.; Boulet, G.; Williams, D.G. Using the dual approach of FAO-56 for partitioning ET into soil and plant components for olive orchards in a semi-arid region. *Agric. Water Manag.* **2010**, *97*, 1769–1778. [CrossRef]
21. Sepulcre-Cantó, G.; Zarco-Tejada, P.J.; Jiménez-Muños, J.C.; Sobrino, J.A.; De Miguel, E.; Villalobos, F.J. Detection of water stress in olive orchard with thermal remote sensing imagery. *Agric. For. Meteorol.* **2006**, *136*, 31–44. [CrossRef]
22. Santos, F.L. Assessing olive evapotranspiration partitioning from soil water balance and radiometric soil and canopy temperatures. *Agronomy* **2018**, *8*, 43. [CrossRef]
23. Capraro, F.; Tosetti, S.; Rossomando, F.; Mut, V.; Serman, F.V. Web-Based System for the Remote Monitoring and Management of Precision Irrigation: A Case Study in an Arid Region of Argentina. *Sensors* **2018**, *18*, 3847. [CrossRef] [PubMed]
24. Hoedjes, J.C.B.; Chehbouni, A.; Jacob, F.; Ezzahar, J.; Boulet, G. Deriving daily evapotranspiration from remotely sensed instantaneous evaporative fraction over olive orchard in semi-arid Morocco. *J. Hydrol.* **2008**, *354*, 53–64. [CrossRef]
25. Minacapilli, M.; Agnese, C.; Blanda, F.; Cammalleri, C.; Ciraolo, G.; D'Urso, G.; Iovino, M.; Pumo, D.; Provenzano, G.; Rallo, G. Estimation of actual evapotranspiration of Mediterranean perennial crops by means of remote-sensing based surface energy balance models. *Hydrol. Earth Syst. Sci.* **2009**, *13*, 1061–1074. [CrossRef]
26. Santos, C.; Lorite, I.J.; Allen, R.G.; Tasumi, M. Aerodynamic parameterization of the satellite-based energy balance (METRIC) model for ET estimation in rainfed olive orchards of Andalusia, Spain. *Water Resour. Manag.* **2012**, *26*, 3267–3283. [CrossRef]
27. Pôças, I.; Paço, T.A.; Cunha, M.; Andrade, J.A.; Silvestre, J.; Sousa, A.; Santos, F.L.; Pereira, L.S.; Allen, R.G. Satellite based evapotranspiration of a super-intensive olive orchard: Application of METRIC algorithm. *Biosyst. Eng.* **2014**, *128*, 69–81. [CrossRef]
28. Pôças, I.; Paço, T.A.; Paredes, P.; Cunha, M.; Pereira, L.S. Estimation of actual crop coefficients using remotely sensed vegetation indices and soil water balance modelled data. *Remote Sens.* **2015**, *7*, 2373–2400. [CrossRef]
29. Ortega-Farías, S.; Ortega-Salazar, S.; Poblete, T.; Kilic, A.; Allen, R.G.; Poblete-Echeverría, C.; Ahumada-Orellana, L.; Zuñiga, M.; Sepúlveda, D. Estimation of energy balance components over a drip-irrigated olive orchard using thermal and multispectral cameras placed on a helicopter-based unmanned aerial vehicle (UAV). *Remote Sens.* **2016**, *8*, 638. [CrossRef]
30. Abazi, U.; Lorite, I.J.; Cárceles, B.; Martínez Raya, A.; Durán, V.H.; Francia, J.R.; Gómez, J.A. WABOL: A conceptual water balance model for analyzing rainfall water use in olive orchards under different soil and cover crop management strategies. *Comput. Electron. Agric.* **2013**, *91*, 35–48. [CrossRef]
31. Autovino, D.; Rallo, G.; Provenzano, G. Predicting soil and plant water status dynamic in olive orchards under different irrigation systems with Hydrus-2D: Model performance and scenario analysis. *Agric. Water Manag.* **2018**, *203*, 225–235. [CrossRef]
32. Pereira, L.S.; Allen, R.G.; Smith, M.; Raes, D. Crop evapotranspiration estimation with FAO56: Past and future. *Agric. Water Manag.* **2015**, *147*, 4–20. [CrossRef]
33. Allen, R.G.; Pereira, L.S.; Smith, M.; Raes, D.; Wright, J. FAO-56 Dual Crop Coefficient Method for Estimating Evaporation from Soil and Application Extensions. *J. Irrig. Drain. Eng.* **2005**, *131*, 2–13. [CrossRef]
34. Rosa, R.D.; Paredes, P.; Rodrigues, G.C.; Alves, I.; Fernando, R.M.; Pereira, L.S.; Allen, R.G. Implementing the dual crop coefficient approach in interactive software. 1. Background and computational strategy. *Agric. Water Manag.* **2012**, *103*, 8–24. [CrossRef]
35. Fandiño, M.; Cancela, J.J.; Rey, B.J.; Martínez, E.M.; Rosa, R.G.; Pereira, L.S. Using the dual-Kc approach to model evapotranspiration of albariño vineyards (*Vitis vinifera* L. cv. albariño) with consideration of active ground cover. *Agric. Water Manag.* **2012**, *112*, 75–87. [CrossRef]
36. Paredes, P.; Rodrigues, G.C.; Alves, I.; Pereira, L.S. Partitioning evapotranspiration, yield prediction and economic returns of maize under various irrigation management strategies. *Agric. Water Manag.* **2014**, *135*, 27–39. [CrossRef]
37. Pereira, L.S.; Paredes, P.; Rodrigues, G.C.; Neves, M. Modeling malt barley water use and evapotranspiration partitioning in two contrasting rainfall years. Assessing AquaCrop and SIMDualKc models. *Agric. Water Manag.* **2015**, *159*, 239–254, Corrigendum in **2015**, *163*, 408. [CrossRef]

38. Paço, T.A.; Ferreira, M.I.; Rosa, R.G.; Paredes, P.; Rodrigues, G.; Conceição, N.; Pacheco, C.; Pereira, L.S. The dual crop coefficient approach using a density factor to simulate the evapotranspiration of a peach orchard: SIMDualKc model versus eddy covariance measurements. *Irrig. Sci.* **2012**, *30*, 115–126. [CrossRef]
39. Ran, H.; Kang, S.; Li, F.; Tong, L.; Ding, R.; Du, T.; Li, S.; Zhang, X. Performance of AquaCrop and SIMDualKc models in evapotranspiration partitioning on full and deficit irrigated maize for seed production under plastic film-mulch in an arid region of China. *Agric. Syst.* **2017**, *151*, 20–32. [CrossRef]
40. Zhao, N.; Liu, Y.; Cai, J.; Paredes, P.; Rosa, R.D.; Pereira, L.S. Dual crop coefficient modelling applied to the winter wheat-summer maize crop sequence in North China Plain: Basal crop coefficients and soil evaporation component. *Agric. Water Manag.* **2013**, *117*, 93–105. [CrossRef]
41. Gao, Y.; Yang, L.; Shen, X.; Li, X.; Sun, J.; Duan, A.; Wu, L. Winter wheat with subsurface drip irrigation (SDI): Crop coefficients, water-use estimates and effects of SDI on grain yield and water use efficiency. *Agric. Water Manag.* **2014**, *146*, 1–10. [CrossRef]
42. Wei, Z.; Paredes, P.; Liu, Y.; Chi, W.-W.; Pereira, L.S. Modelling transpiration, soil evaporation and yield prediction of soybean in North China Plain. *Agric. Water Manag.* **2015**, *147*, 43–53. [CrossRef]
43. Allen, R.G.; Pereira, L.S. Estimating crop coefficients from fraction of ground cover and height. *Irrig. Sci.* **2009**, *28*, 17–34. [CrossRef]
44. Kottek, M.; Grieser, J.; Beck, C.; Rudolf, B.; Rubel, F. World Map of the Köppen-Geiger climate classification updated. *Meteorol. Z.* **2006**, *15*, 259–263. [CrossRef]
45. IUSS; Working Group WRB. World Reference Base for Soil Resources 2014, Update 2015. In *International Soil Classification System for Naming Soils and Creating Legends for Soil Maps*; World Soil Resources Reports No. 106; FAO: Rome, Italy, 2015; 192p.
46. Fandiño, M.; Olmedo, J.L.; Martínez, E.M.; Valladares, J.; Paredes, P.; Rey, B.J.; Mota, M.; Cancela, J.J.; Pereira, L.S. Assessing and modelling water use and the partition of evapotranspiration of irrigated hop (*Humulus lupulus*) and relations of transpiration with hops yield and alpha-acids. *Ind. Crop Prod.* **2015**, *77*, 204–217. [CrossRef]
47. Ferreira, M.I.; Paço, T.A.; Silvestre, J. Combining techniques to study evapotranspiration in woody crops: Application to small areas—Two case studies. *Acta Hortic. ISHS* **2004**, *664*, 225–232. [CrossRef]
48. Mauder, M.; Foken, T. Documentation and Instruction Manual of the Eddy-Covariance Software Package TK3 (Update). Arbeitsergebnisse Nr. 62; 2015 Univ Bayreuth, Abt Mikrometeorol. Available online: https://epub.uni-bayreuth.de/2130/1/ARBERG062.pdf (accessed on 5 July 2017).
49. Foken, T.; Leuning, R.; Oncley, S.P.; Mauder, M.; Aubinet, M. Corrections and data quality. In *Eddy Covariance: A Practical Guide to Measurement and Data Analysis*; Aubinet, M., Vesala, T., Papale, D., Eds.; Springer: Berlin/Heidelberg, Germany, 2011.
50. Vickers, D.; Mahrt, L. Quality control and flux sampling problems for tower and aircraft data. *J. Atmos. Ocean. Technol.* **1997**, *14*, 512–526. [CrossRef]
51. Kaimal, J.C.; Finnigan, J.J. *Atmospheric Boundary Layer Flows: Their Structure and Measurement*; Oxford University Press: New York, NY, USA, 1994.
52. Tanner, B.D.; Swiatek, E.; Greene, J.P. Density fluctuations and use of the krypton hygrometer in surface flux measurements. In *Management of Irrigation and Drainage Systems: Integrated Perspectives*; Allen, R.G., Ed.; American Society of Civil Engineers: New York, NY, USA, 1993; pp. 945–952.
53. Moore, C.J. Frequency-response corrections for eddy-correlation systems. *Bound.-Layer Meteorol.* **1986**, *37*, 17–35. [CrossRef]
54. Schotanus, P.; Nieuwstadt, F.T.M.; Debruin, H.A.R. Temperature-measurement with a sonic anemometer and its application to heat and moisture fluxes. *Bound.-Layer Meteorol.* **1983**, *26*, 81–93. [CrossRef]
55. Webb, E.K.; Pearman, G.I.; Leuning, R. Correction of flux measurements for density effects due to heat and water-vapor transfer. *Q. J. R. Meteorol. Soc.* **1980**, *106*, 85–100. [CrossRef]
56. Schuepp, P.H.; Leclerc, M.Y.; Macpherson, J.I.; Desjardins, R.L. Footprint prediction of scalar fluxes from analytical solutions of the diffusion equation. *Bound.-Layer Meteorol.* **1990**, *50*, 355–373. [CrossRef]
57. Testi, L.; Villalobos, F.J.; Orgaz, F. Evapotranspiration of a young irrigated olive orchard in southern Spain. *Agric. For. Meteorol.* **2004**, *121*, 1–18. [CrossRef]
58. Teixeira, A.H.D.C.; Bastiaanssen, W.G.M.; Moura, M.S.B.; Soares, J.M.; Ahmad, M.D.; Bos, M.G. Energy and water balance measurements for water productivity analysis in irrigated mango trees, Northeast Brazil. *Agric. For. Meteorol.* **2008**, *148*, 1524–1537. [CrossRef]

59. Conceição, N.; Tezza, L.; Häusler, M.; Lourenço, S.; Pacheco, C.A.; Ferreira, M.I. Three years of monitoring evapotranspiration components and crop and stress coefficients in a deficit irrigated intensive olive orchard. *Agric. Water Manag.* **2017**, *191*, 138–152. [CrossRef]
60. Granier, A. Une nouvelle méthode pour la mesure du flux de sève brute dans le tronc des arbres. *Ann. Sci. For.* **1985**, *42*, 193–200. [CrossRef]
61. Silva, R.M.; Paço, T.A.; Ferreira, M.I.; Oliveira, M. Transpiration of a kiwifruit orchard estimated using the Granier sap flow method calibrated under field conditions. *Acta Hortic. ISHS* **2008**, *792*, 593–600. [CrossRef]
62. Steppe, K.; De Pauw, D.J.W.; Doody, T.M.; Teskey, R.O. A comparison of sap flux density using thermal dissipation, heat pulse velocity and heat field deformation methods. *Agric. For. Meteorol.* **2010**, *150*, 1046–1056. [CrossRef]
63. Bush, S.E.; Hultine, K.R.; Sperry, J.S.; Ehleringer, J.R. Calibration of thermal dissipation sap flow probes for ring- and diffuse-porous trees. *Tree Physiol.* **2010**, *30*, 1545–1554. [CrossRef]
64. Hölttä, T.; Linkosalo, T.; Riikonen, A.; Sevanto, S.; Nikinmaa, E. An analysis of Granier sap flow method, its sensitivity to heat storage and a new approach to improve its time dynamics. *Agric. For. Meteorol.* **2015**, *211–212*, 2–12. [CrossRef]
65. Marañón-Jiménez, S.; Van den Bulcke, J.; Piayda, A.; Van Acker, J.; Cuntz, M.; Rebmann, C.; Steppe, K. X-ray computed microtomography characterizes the wound effect that causes sap flow underestimation by thermal dissipation sensors. *Tree Physiol.* **2017**, *38*, 288–302. [CrossRef]
66. Ritchie, J.T. Model for predicting evaporation from a row crop with incomplete cover. *Water Resour. Res.* **1972**, *8*, 1204–1213. [CrossRef]
67. Paço, T.A.; Conceição, N.; Ferreira, M.I. Measurements and estimates of peach orchard evapotranspiration in Mediterranean conditions. *Acta Hortic.* **2004**, *664*, 505–512. [CrossRef]
68. Paço, T.A.; Conceição, N.; Ferreira, M.I. Peach orchard evapotranspiration in a sandy soil: Comparison between eddy covariance measurements and estimates by the FAO 56 approach. *Agric. Water Manag.* **2006**, *85*, 305–313. [CrossRef]
69. López-Olivari, R.; Ortega-Farías, S.; Poblete-Echeverría, C. Partitioning of net radiation and evapotranspiration over a superintensive drip-irrigated olive orchard. *Irrig. Sci.* **2016**, *34*, 17–31. [CrossRef]
70. Tukey, J.W. *Exploratory Data Analysis*; Addison-Wesley: Reading, MA, USA, 1977.
71. Liu, Y.; Pereira, L.S.; Fernando, R.M. Fluxes through the bottom boundary of the root zone in silty soils: Parametric approaches to estimate groundwater contribution and percolation. *Agric. Water Manag.* **2006**, *84*, 27–40. [CrossRef]
72. Allen, R.G.; Wright, J.L.; Pruitt, W.O.; Pereira, L.S.; Jensen, M.E. Water requirements. In *Design and Operation of Farm Irrigation Systems*, 2nd ed.; Hoffman, G.J., Evans, R.G., Jensen, M.E., Martin, D.L., Elliot, R.L., Eds.; ASABE: St. Joseph, MI, USA, 2007; pp. 208–288.
73. Zhang, B.; Liu, Y.; Xu, D.; Zhao, N.; Lei, B.; Rosa, R.D.; Paredes, P.; Paco, T.A.; Pereira, L.S. The dual crop coefficient approach to estimate and partitioning evapotranspiration of the winter wheat-summer maize crop sequence in North China Plain. *Irrig. Sci.* **2013**, *31*, 1303–1316. [CrossRef]
74. Tian, F.; Yang, P.; Hu, H.; Dai, C. Partitioning of cotton field evapotranspiration under mulched drip irrigation based on a dual crop coefficient model. *Water* **2016**, *8*, 72. [CrossRef]
75. Rosa, R.D.; Paredes, P.; Rodrigues, G.C.; Fernando, R.M.; Alves, I.; Pereira, L.S.; Allen, R.G. Implementing the dual crop coefficient approach in interactive software: 2. Model testing. *Agric. Water Manag.* **2012**, *103*, 62–77. [CrossRef]
76. Zhang, H.; Huang, G.; Xu, X.; Xiong, Y.; Huang, Q. Estimating evapotranspiration of processing tomato under plastic mulch using the SIMDualKc model. *Water* **2018**, *10*, 1088. [CrossRef]
77. Nash, J.E.; Sutcliffe, J.V. River flow forecasting through conceptual models: Part 1. A discussion of principles. *J. Hydrol.* **1970**, *10*, 282–290. [CrossRef]
78. Moriasi, D.N.; Arnold, J.G.; Van Liew, M.W.; Bingner, R.L.; Harmel, R.D.; Veith, T.L. Model evaluation guidelines for systematic quantification of accuracy in watershed simulations. *Trans. ASABE* **2007**, *50*, 885–900. [CrossRef]
79. Rallo, G.; Baiamonte, G.; Manzano Juárez, J.; Provenzano, G. Improvement of FAO-56 model to estimate transpiration fluxes of drought tolerant crops under soil water deficit: Application for olive groves. *J. Irrig. Drain. Eng.* **2014**, *140*, A4014001. [CrossRef]

80. Testi, L.; Orgaz, F.; Villalobos, F.J. Variations in bulk canopy conductance of an irrigated olive (*Olea europaea* L.) orchard. *Environ. Exp. Bot.* **2006**, *55*, 15–28. [CrossRef]
81. Martínez-Cob, A.; Faci, J.M. Evapotranspiration of an hedge-pruned olive orchard in a semiarid area of NE Spain. *Agric. Water Manag.* **2010**, *97*, 410–418. [CrossRef]
82. Fernández, J.E.; Moreno, F. Water Use by the Olive Tree. *J. Crop Prod.* **2000**, *2*, 101–162. [CrossRef]